MOX-Report No. 10/2016

A review of the XFEM-based approximation of flow in fractured porous media

Flemisch, B.; Fumagalli, A.; Scotti, A.

MOX, Dipartimento di Matematica
Politecnico di Milano, Via Bonardi 9 - 20133 Milano (Italy)

mox-dmat@polimi.it http://mox.polimi.it

A review of the XFEM-based approximation of flow in fractured porous media

Bernd Flemisch · Alessio Fumagalli · Anna Scotti

Abstract This paper presents a review of the available mathematical models and corresponding non-conforming numerical approximations which describe single-phase fluid flow in a fractured porous medium. One focus is on the geometrical difficulties that may arise in realistic simulations such as intersecting and immersed fractures. Another important aspect is the choice of the approximation spaces for the discrete problem: in mixed formulations, both the Darcy velocity and the pressure are considered as unknowns, while in classical primal formulations, a richer space for the pressure is considered and the Darcy velocity is computed a posteriori. In both cases, the extended finite element method is used, which allows for a complete geometrical decoupling among the fractures and rock matrix grids. The fracture geometries can thus be independent of the underlying grid thanks to suitable enrichments of the spaces that are able to represent possible jumps of the solution across the

B. Flemisch
Department of Hydromechanics and Modelling of Hydrosystems
University of Stuttgart
Pfaffenwaldring 61
70569 Stuttgart, Germany
Tel.: +49-711-68569162
E-mail: bernd@iws.uni-stuttgart.de

A. Fumagalli
Department of Mathematics
University of Bergen
Realfagbygget, Allégt. 41
5020 Bergen, Norway
E-mail: alessio.fumagalli@uib.no

A. Scotti
MOX– Modellistica e Calcolo Scientifico
Dipartimento di Matematica "F. Brioschi"
Politecnico di Milano
via Bonardi 9, 20133 Milano, Italy
E-mail: anna.scotti@polimi.it

fractures. Finally, due to the dimensional reduction, a better approximation of the resulting boundary conditions for the fractures is addressed.

Keywords Fractured porous media · Reduced Model · XFEM

1 Introduction

The simulation of subsurface flow is of great importance for a large number of applications ranging from the production of energy (oil and gas reservoirs, geothermal energy) to the management of water resources, or the safe storage of atomic waste and carbon dioxide. Fractures are present in porous media at a variety of scales. Large fractures and faults in particular are very relevant for the flow since they can either act as barriers (in the case of impermeable faults) or preferential pathways for the flow (in the case of permeable fractures). Opposed to small-scale fractures, that can be accounted for by upscaling of the permeability, large features should be explicitly included in the model to reproduce their non-local effects on the flow. Thanks to the developments of numerical methods and computing power direct numerical simulations of fracture networks are replacing or complementing multi-continua approaches such as dual-porosity/permeability.

Fractures and faults are three-dimensional regions characterized by a different porosity and permeability with respect to the surrounding porous matrix. However, thanks to their small aperture compared to the typical length and the size of the domain, they are usually represented as $(N-1)$-dimensional interfaces immersed in a N-dimensional matrix. From a computational viewpoint, this avoids the need for an extremely fine grid to resolve the width of fractures, that are now replaced by discontinuity surfaces where a suitable reduced $(N-1)$-dimensional problem is solved and coupled with the surrounding flow. However, the complexity of geological structures remains one of the main challenges in large-scale numerical simulations. Indeed, the data for the construction of the model are usually given as a lage number of possibly intersecting surfaces, called horizons, that separate layers with different mechanic and hydraulic properties, and a set of surfaces that represent faults and fractures. In this framework, the construction of a grid which is conforming with all the aforementioned features is a difficult task, [21], whose outcome could be a grid that is either too refined to be used, or with low quality elements. Since in these realistic cases the construction of a high-quality grid that honors the geometry of hundreds or thousands of fractures is a challenging task, two alternative approaches are possible:

- to develop numerical methods that are accurate and robust even for very distorted grids, such as the Mimetic Finite Difference Methods [8],
- to allow the fractures to cross a fairly regular and coarse grid in arbitrary ways, and to employ the eXtended Finite Element Method (XFEM) to account for the solution discontinuities within elements.

This paper presents the second approach, reviewing the recent literature on the application of the XFEM to the simulation of flow in fractured porous media, focusing on single-phase flow in the presence of one or more, possibly intersecting, fractures.

The XFEM has been successfully used for the simulation of crack mechanics for a long time, [23,24,48], while its application to flow in fractured media is a recent development. Allowing for non-matching grids with respect to the fracture network can be advantageous in geological problems since not only it avoids the burden of computing a conforming grid, but it avoids the need for re-meshing in the case of uncertain geometry, i.e. one could perform simulations of different scenarios with different fracture configurations with the same background grid.

The enrichment of the finite element spaces should be able to effectively represent discontinuities in the pressure and in the flux across fractures: pressure jumps arise in the case of impermeable interfaces, while a discontinuous flux can be observed due to the fact that fluid can enter the fractures and flow along them.

The development and the analysis of $(N-1)$-dimensional models for fractures for single-phase flow have been extensively addressed in [2,46,7,30,13], where the fracture flow equations and the proper interface conditions across the fracture have been first derived, and the continuous and discrete problems have been studied in their mixed formulation. However, in the aforementioned works, the computational grid of the porous domain is considered to be matching with the fracture, i.e. the fracture is the (conforming) interface between two mesh blocks, possibly with different resolution. Similarly, in more recent works, this type of space discretization has been employed to describe the flow in faulted sedimentary basins, coupled with a double-layer model for the fault, see [56,27]. However, while non-conforming meshes on the interface could be dealt with by mortaring, this does not allow the fractures to cut the elements of the grid.

The use of XFEM to deal with fractures as non-matching, immersed interfaces, was first introduced in 2011, for the single phase case, in [44,19]. In the former, the concept of EFEM (Enriched Finite Element Method) is applied to the primal formulation with suitable enrichments for the pressure, while in the latter the mixed formulation of the problem is considered, and the authors employ concepts borrowed from [40] to enrich both the pressure and the Darcy velocity spaces. In the same years, XFEM have been applied for the discretization of the primal formulation in [54].

The application to the case of several intersecting fractures is discussed in [28,11] in the case of an impervious surrounding medium, with slightly different coupling conditions at the intersections based on different assumptions on the fractures permeability. The coupled problem, in the mixed and primal formulation respectively, are considered in [31,32,55]. As concerns the physics of flow in porous media, some works consider also the case of passive transport of solutes in fractured porous media, [34], and two-phase flow [35] by means

of the XFEM. Moreover, the coupling of Darcy flow with fracture mechanics (opening, propagation) is addressed in [39,52].

Regarding the analysis of the method, the inf-sup stability of XFEM applied to Darcy flow in porous media has been proven, under suitable conditions, in [19,22].

This paper is organized as follows. In Section 2, we introduce the mathematical model for single-phase flow in fractured porous media in the equi-dimensional case, and derive the corresponding hybrid-dimensional, or reduced, model. Intersecting fractures are considered, as well as the task of assigning boundary conditions for the fractures. In Section 3, we present the numerical discretization techniques for the problem in primal and dual mixed form, with a focus on the ad-hoc enrichments at intersections and tips, and on the approximation of coupling terms. Section 4 is dedicated to solvers for the resulting linear system, in particular to conditioning issues and the choice of iterative vs. monolithic approaches. Finally, Section 5 is devoted to some concluding remarks and future perspectives.

2 Governing equations

In this section, we present the mathematical model of single-phase flow in porous media, focusing our attention on the description of the fractures. We start considering the standard Darcy law and mass balance in an equi-dimensional setting, where the fractures are N-dimensional regions embedded in an N-dimensional porous matrix. Then we introduce the so called reduced, or hybrid-dimensional, models to handle fractures as objects of effective lower dimension, intersections and branching of fractures, and proper boundary conditions to prescribe at the fracture tips and on the cut matrix boundaries.

2.1 Equi-dimensional models

We consider an inert and at rest porous medium which can be modeled as a bounded, connected, and open set $\mathcal{D} \subset \mathbb{R}^N$, N=2 or 3. We assume that the medium is saturated with a single incompressible fluid phase that is composed of a unique component, e.g., water. The boundary, which is required to be regular enough for the forthcoming assumptions, is indicated by $\partial\mathcal{D}$ with outward unit normal $\boldsymbol{n}_{\mathcal{D}}$. Let us assume that $\mathcal{D}$ contains several fractures, that all together constitute a single domain Γ of spatial dimension N such that $\Gamma \subset \mathcal{D}$, which is a possibly unconnected, open subset of $\mathcal{D}$. The fracture network can also be seen as the union of fracture branches Γ_i. The surrounding porous rock, namely, the remaining part of $\mathcal{D}$, is called $\Omega := \mathcal{D} \setminus \overline{\Gamma}$. The outer boundary of the rock matrix is indicated by $\partial\Omega = \overline{\Omega} \cap \partial\mathcal{D}$, while the outer boundary of the fracture network is indicated by $\partial\Gamma$ and defined by $\partial\Gamma := \overline{\Gamma} \cap \partial\mathcal{D}$. Moreover, the internal part of the fracture boundary, namely, the interface between the fracture domain and the surrounding medium, is indicated by γ and defined

as $\gamma := \overline{\Gamma} \cap \overline{\Omega}$. For each fracture branch, we call its own part of this internal boundary γ_i. The unit normal, pointing out of Γ into Ω, is indicated by $\boldsymbol{n}$. We suppose that for each fracture branch there exists a central axis $\hat{\gamma}_i$, which is a non self-intersecting $(N-1)$-dimensional surface, such that a fracture branch can be described as

$$\Gamma_i = \left\{ \boldsymbol{x} \in \mathbb{R}^N : \boldsymbol{x} = \boldsymbol{s} + r\boldsymbol{n}_i,\ \boldsymbol{s} \in \hat{\gamma}_i,\ |r| < \frac{d_i}{2} \right\}, \tag{1}$$

where d_i is the aperture of Γ_i, which may depend on the curvilinear abscissa $\boldsymbol{s}$, and $\boldsymbol{n}_i$ is the unit normal associated with the central axis $\hat{\gamma}_i$. We assume that the apertures d_i are small compared to other characteristic dimensions of the fractures. With definition (1) the fracture domain is composed by $\overline{\Gamma} = \cup\overline{\Gamma_i}$, but note that Γ_i may intersect each other with a non-null intersection. See Figure 1 for an illustration of the aforementioned notation.

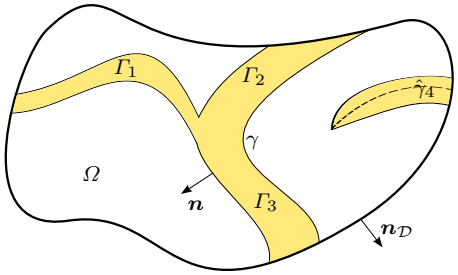

Fig. 1: Notation for a general configuration of fractures in the equi-dimensional model.

In this work we assume that the fractures are filled by a porous medium themselves such that Darcy flow takes place in both the rock matrix and fractures. In the relevant case of open fractures the lubrication model could be used, see for instance [57].

2.1.1 Dual formulation

In this part, our objective is to compute the steady-state pressure field p and the Darcy velocity field, or macroscopic velocity, $\boldsymbol{u}$ in the entire porous domain $\mathcal{D}$. To this purpose, following for example [9], we employ the law of mass conservation together with Darcy's law and, to ease the notation, we assume homogeneous boundary conditions for the pressure on the whole boundary. The system of equations for the porous matrix Ω is given by

$$\begin{cases} \nabla \cdot \boldsymbol{u} = f \\ \boldsymbol{u} + \Lambda \nabla p = \boldsymbol{0} & \text{in } \Omega, \\ p = 0 & \text{on } \partial\Omega, \end{cases} \tag{2a}$$

where the scalar source term f represents a possible volume source or sink and Λ denotes the symmetric and positive definite permeability tensor in Ω. To simplify the notation we consider a permeability tensor that is already scaled with the viscosity. Coupled with (2a), a similar system of equations can be considered for the fracture network. The data and unknowns related to the fractures are indicated with a subscript f. We obtain

$$\begin{cases} \nabla \cdot \boldsymbol{u}_{\mathrm{f}} = f_{\mathrm{f}} & \\ \boldsymbol{u}_{\mathrm{f}} + \Lambda_{\mathrm{f}} \nabla p_{\mathrm{f}} = \boldsymbol{0} & \text{in } \Gamma, \\ p_{\mathrm{f}} = 0 & \text{on } \partial\Gamma. \end{cases} \tag{2b}$$

Following [46] we require that the permeability tensor in the fracture system, for each fracture branch, can be written as $\Lambda_{\mathrm{f},i} = \lambda_{i,\boldsymbol{n}} \boldsymbol{N}_i + \lambda_{i,\boldsymbol{\tau}} \boldsymbol{T}_i$, where the projection matrix $\boldsymbol{N}_i$ in the direction normal to $\hat{\gamma}_i$ and the projection matrix $\boldsymbol{T}_i$ in the direction tangential to $\hat{\gamma}_i$ are defined as follows:

$$\boldsymbol{N}_i := \boldsymbol{n}_i \otimes \boldsymbol{n}_i \quad \text{and} \quad \boldsymbol{T}_i := \boldsymbol{I} - \boldsymbol{N}_i.$$

To couple the systems (2a) and (2b) we consider the following classical interface conditions, namely

$$\begin{cases} p = p_{\mathrm{f}} & \\ \boldsymbol{u} \cdot \boldsymbol{n} = \boldsymbol{u}_{\mathrm{f}} \cdot \boldsymbol{n} & \text{on } \gamma. \end{cases} \tag{2c}$$

Combining (2a), (2b) and (2c), we obtain the strong problem formulation in its dual form.

Problem 1 (Dual equi-dimensional strong formulation) Find velocity fields $\boldsymbol{u}, \boldsymbol{u}_{\mathrm{f}}$ and pressure fields p, p_{f} such that (2) is fulfilled.

The proof of the well-posedness of Problem 1 in its mixed weak form can be found in a number of references, such as [15,50,25,53].

2.1.2 Primal formulation

A common formulation for single-phase porous-media flow is the so-called primal formulation, that can be obtained inserting Darcy's law for matrix and fracture domain, namely, the second lines of (2a), (2b) into the mass-balance equations, namely, the first lines of (2a), (2b), as well as into the flux-coupling condition, namely, the second line of (2c). In particular, for the matrix domain Ω, we obtain

$$\begin{cases} -\nabla \cdot (\Lambda \nabla p) = f & \text{in } \Omega, \\ p = 0 & \text{on } \partial\Omega, \end{cases} \tag{3a}$$

while for the fracture domain Γ, we have

$$\begin{cases} -\nabla \cdot (\Lambda_{\mathrm{f}} \nabla p_{\mathrm{f}}) = f_{\mathrm{f}} & \text{in } \Gamma, \\ p_{\mathrm{f}} = 0 & \text{on } \partial\Gamma, \end{cases} \tag{3b}$$

coupled by

$$\begin{cases} p = p_{\mathrm{f}} \\ \Lambda \nabla p \cdot \boldsymbol{n} = \Lambda_{\mathrm{f}} \nabla p_{\mathrm{f}} \cdot \boldsymbol{n} \end{cases} \quad \text{on } \gamma. \tag{3c}$$

The problem can, in this case, be cast as follows.

Problem 2 (Primal equi-dimensional strong formulation) Find pressure fields p, p_{f} such that (3) is fulfilled.

The well-posedness of Problem 2 and its weak form can be found in any standard textbook on partial differential equations or finite elements.

2.2 Hybrid-dimensional models

In this section, we present the hybrid-dimensional model, or reduced model, in the case of single fracture dividing the domain in two unconnected parts. We

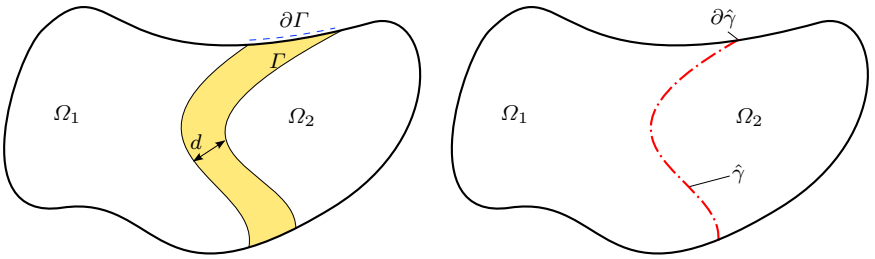

(a) Equi-dimensional model domain.

(b) Hybrid-dimensional model domain which includes a lower dimensional fracture.

Fig. 2: Model domains with fracture.

refer to [4,26,6,46,20] for a detailed presentation. The derivation of the model is based on its dual formulation, however, we present also its primal formulation, obtained with a "post-processing". For both formulations, we briefly introduce their weak formulation to be used for the numerical discretization.

During the process, we substitute the fracture Γ by its centre line $\hat{\gamma}$ and the surrounding porous medium is enlarged to fill the gap. In practical cases, this step is very seldom performed since the fracture geometry is directly given as an object of codimension one. The Darcy equations (2a) for the rock matrix are thus the same as in the equi-dimensional case and we focus only on the equations (2b) for the fracture. Since Ω is split in two parts $\Omega_{1,2}$, we define $\boldsymbol{n} = \boldsymbol{n}_1 = -\boldsymbol{n}_2$, where $\boldsymbol{n}_i$ is the outward-pointing normal of Ω_i. Let us introduce the normal and tangential divergence and gradient on the fracture:

given two regular functions $\boldsymbol{a}$ and a, respectively vector- and scalar-valued, we define

$$\nabla \cdot \boldsymbol{a} = \nabla_{\boldsymbol{n}} \cdot \boldsymbol{a} + \nabla_{\boldsymbol{\tau}} \cdot \boldsymbol{a} \quad \text{with} \quad \nabla_{\boldsymbol{n}} \cdot \boldsymbol{a} := \boldsymbol{N} : \nabla \boldsymbol{a} \quad \text{and} \quad \nabla_{\boldsymbol{\tau}} \cdot \boldsymbol{a} := \boldsymbol{T} : \nabla \boldsymbol{a},$$
$$\nabla a = \nabla_{\boldsymbol{n}} a + \nabla_{\boldsymbol{\tau}} a \quad \text{with} \quad \nabla_{\boldsymbol{n}} a := \boldsymbol{N} \nabla a \quad \text{and} \quad \nabla_{\boldsymbol{\tau}} a := \boldsymbol{T} \nabla a.$$

2.2.1 Dual formulation

We decompose the Darcy velocity in the fracture into its normal part $\boldsymbol{u}_{\mathrm{f},\boldsymbol{n}} := \boldsymbol{N}\boldsymbol{u}_{\mathrm{f}}$ and tangential part $\boldsymbol{u}_{\mathrm{f},\boldsymbol{\tau}} := \boldsymbol{T}\boldsymbol{u}_{\mathrm{f}}$, such that $\boldsymbol{u}_{\mathrm{f}} = \boldsymbol{u}_{\mathrm{f},\boldsymbol{n}} + \boldsymbol{u}_{\mathrm{f},\boldsymbol{\tau}}$. We consider first the conservation equation which is integrated along the normal direction of $\hat{\gamma}$ for the fracture aperture d. We obtain a conservation equation in the tangential space of $\hat{\gamma}$ for the reduced flux $\hat{\boldsymbol{u}} := \int_{-d/2}^{d/2} \boldsymbol{u}_{\mathrm{f},\boldsymbol{\tau}}$ which involves also the contribution of the incoming flux from the surrounding porous medium, namely,

$$\nabla_{\boldsymbol{\tau}} \cdot \hat{\boldsymbol{u}} = \hat{f} + [\![\boldsymbol{u} \cdot \boldsymbol{n}]\!]_{\hat{\gamma}} \quad \text{in } \hat{\gamma}, \tag{4}$$

where the reduced source term is defined as $\hat{f} := \int_{-d/2}^{d/2} f_{\mathrm{f}}$. In (4) we made use of the jump operator defined as $[\![\boldsymbol{u} \cdot \boldsymbol{n}]\!]_{\hat{\gamma}} := \boldsymbol{u}_1 \cdot \boldsymbol{n} - \boldsymbol{u}_2 \cdot \boldsymbol{n}$, with an abuse of notation for the normal $\boldsymbol{n}$. We consider now the Darcy equation projected on the tangential space of $\hat{\gamma}$ and integrated in normal direction for the aperture of the fracture, obtaining

$$\hat{\boldsymbol{u}} + \hat{\lambda} \nabla_{\boldsymbol{\tau}} \hat{p} = \boldsymbol{0} \quad \text{in } \hat{\gamma}, \tag{5}$$

where $\hat{p}$ is the reduced pressure in the fracture, defined as $\hat{p} := \frac{1}{d} \int_{-d/2}^{d/2} p_{\mathrm{f}}$. In the previous equation, $\hat{\lambda}$ is the effective permeability in tangential direction, defined as $\hat{\lambda} := d\lambda_{\mathrm{f},\boldsymbol{\tau}}$. Finally, projecting Darcy's law on the normal space of the fracture and integrating in normal direction on the first and on the second half of the aperture, we end up with coupling conditions between the lower-dimensional fracture and the rock matrix. Using a suitable approximation of the integral of $\boldsymbol{u}_i \cdot \boldsymbol{n}$, as discussed in [46, 7], we get

$$\begin{cases} \xi \boldsymbol{u}_1 \cdot \boldsymbol{n} + (1-\xi) \boldsymbol{u}_2 \cdot \boldsymbol{n} = 2\lambda_{\hat{\gamma}} (p_1 - \hat{p}) \\ \xi \boldsymbol{u}_2 \cdot \boldsymbol{n} + (1-\xi) \boldsymbol{u}_1 \cdot \boldsymbol{n} = 2\lambda_{\hat{\gamma}} (\hat{p} - p_2) \end{cases} \quad \text{on } \hat{\gamma}, \tag{6}$$

where $\lambda_{\hat{\gamma}}$ is the effective permeability in normal direction of the fracture, defined as $\lambda_{\hat{\gamma}} := \lambda_{\mathrm{f},\boldsymbol{n}}/d$. Moreover, $\xi \in (0.5, 1]$ is a closure parameter related to the pressure cross profile in the fracture, see the aforementioned works for more details. Considering (2a) coupled with (4), (5), and (6) we obtain the following hybrid-dimensional problem.

Problem 3 (Dual hybrid-dimensional strong formulation) Find $(\boldsymbol{u}_i, p_i)$ for $i = 1, 2$ and $(\hat{\boldsymbol{u}}, \hat{p})$ such that

$$\begin{cases} \nabla \cdot \boldsymbol{u}_i = f_i \\ \boldsymbol{u}_i + \Lambda_i \nabla p_i = \boldsymbol{0} \\ p_i = 0 \end{cases} \begin{array}{ll} \text{in } \Omega_i, \\ \\ \text{on } \partial\Omega_i, \end{array} \quad \text{and} \quad \begin{cases} \nabla_{\boldsymbol{\tau}} \cdot \hat{\boldsymbol{u}} = \hat{f} + [\![\boldsymbol{u} \cdot \boldsymbol{n}]\!]_{\hat{\gamma}} \\ \hat{\boldsymbol{u}} + \hat{\lambda} \nabla_{\boldsymbol{\tau}} \hat{p} = \boldsymbol{0} \\ \hat{p} = 0 \end{cases} \begin{array}{ll} \text{in } \hat{\gamma}, \\ \\ \text{on } \partial\hat{\gamma}, \end{array} \tag{7a}$$

with interface conditions

$$\begin{cases} \xi \boldsymbol{u}_1 \cdot \boldsymbol{n} + (1-\xi) \boldsymbol{u}_2 \cdot \boldsymbol{n} = 2\lambda_{\hat{\gamma}} (p_1 - \hat{p}) \\ \xi \boldsymbol{u}_2 \cdot \boldsymbol{n} + (1-\xi) \boldsymbol{u}_1 \cdot \boldsymbol{n} = 2\lambda_{\hat{\gamma}} (\hat{p} - p_2) \end{cases} \quad \text{on } \hat{\gamma}. \tag{7b}$$

An alternative form of the interface conditions (7b), introduced in [18], is

$$\begin{cases} \{\!\{\boldsymbol{u} \cdot \boldsymbol{n}\}\!\}_{\hat{\gamma}} = \lambda_{\hat{\gamma}} [\![p]\!]_{\hat{\gamma}} \\ \xi_0 [\![\boldsymbol{u} \cdot \boldsymbol{n}]\!]_{\hat{\gamma}} = \lambda_{\hat{\gamma}} \left(\{\!\{p\}\!\}_{\hat{\gamma}} - \hat{p} \right) \end{cases} \quad \text{on } \hat{\gamma}, \tag{7b-bis}$$

with $\xi_0 = 4/(2\xi - 1)$ and where we have used the average operators $\{\!\{p\}\!\}_{\hat{\gamma}} := \frac{1}{2}(p_1 + p_2)$ and $\{\!\{\boldsymbol{u} \cdot \boldsymbol{n}\}\!\}_{\hat{\gamma}} := \frac{1}{2}(\boldsymbol{u}_1 \cdot \boldsymbol{n} + \boldsymbol{u}_2 \cdot \boldsymbol{n})$, as well as the jump operator for the pressure $[\![p]\!]_{\hat{\gamma}} := p_1 - p_2$.

We now introduce the weak formulation of the reduced problem, which will be useful to present the XFEM in Section 3. For a detailed presentation of the suitable functional spaces refer to [7]. We start by introducing the following bilinear forms and functionals for the rock matrix

$$\begin{aligned} a_{\mathrm{d}}(\boldsymbol{u}, \boldsymbol{v}) := \sum_i (H \boldsymbol{u}_i, \boldsymbol{v}_i)_{\Omega_i} + \left(\eta_{\hat{\gamma}} \{\!\{\boldsymbol{u} \cdot \boldsymbol{n}\}\!\}_{\hat{\gamma}}, \{\!\{\boldsymbol{v} \cdot \boldsymbol{n}\}\!\}_{\hat{\gamma}} \right)_{\hat{\gamma}} \\ + \xi_0 \left(\eta_{\hat{\gamma}} [\![\boldsymbol{u} \cdot \boldsymbol{n}]\!]_{\hat{\gamma}}, [\![\boldsymbol{v} \cdot \boldsymbol{n}]\!]_{\hat{\gamma}} \right)_{\hat{\gamma}}, \text{ with } i = 1, 2, \end{aligned}$$

with $H := \Lambda^{-1}$, $\eta_{\hat{\gamma}} := \lambda_{\hat{\gamma}}^{-1}$ the inverse of the permeabilities. The bilinear form and the functional which include the source term and possibly boundary conditions read

$$b_{\mathrm{d}}(p, \boldsymbol{v}) := -\sum_i (p_i, \nabla \cdot \boldsymbol{v}_i)_{\Omega_i} \quad \text{and} \quad F(q) := \sum_i (f_i, q_i)_{\Omega_i}.$$

The weak formulation for the fracture requires to introduce the following bilinear forms and functional

$$\hat{a}_{\mathrm{d}}(\hat{\boldsymbol{u}}, \hat{\boldsymbol{v}}) := (\hat{\eta} \hat{\boldsymbol{u}}, \hat{\boldsymbol{v}})_{\hat{\gamma}}, \quad \hat{b}_{\mathrm{d}}(\hat{p}, \hat{\boldsymbol{v}}) := -(\hat{p}, \nabla_{\boldsymbol{\tau}} \cdot \hat{\boldsymbol{v}})_{\hat{\gamma}} \quad \text{and} \quad \hat{F}(\hat{q}) := \left(\hat{f}, \hat{q} \right)_{\hat{\gamma}}.$$

with $\hat{\eta} := \hat{\lambda}^{-1}$ the inverse of the effective tangential permeability. Finally the bilinear form which couples the fracture and the surrounding porous medium

$$c_{\mathrm{d}}(\boldsymbol{u}, \hat{q}) := \left([\![\boldsymbol{u} \cdot \boldsymbol{n}]\!]_{\hat{\gamma}}, \hat{q} \right)_{\hat{\gamma}}.$$

The weak formulation of (7) is given as follows.

Problem 4 (Dual hybrid-dimensional weak formulation) Find $(\boldsymbol{u}_i, p_i)$ for $i = 1, 2$ and $(\hat{\boldsymbol{u}}, \hat{p})$ respecting the given boundary conditions such that

$$\begin{cases} a_{\mathrm{d}}(\boldsymbol{u}, \boldsymbol{v}) + b_{\mathrm{d}}(p, \boldsymbol{v}) + c_{\mathrm{d}}(\hat{p}, \boldsymbol{v}) = 0 \\ b_{\mathrm{d}}(q, \boldsymbol{u}) = F(q) \end{cases} \quad \text{and} \quad \begin{cases} \hat{a}_{\mathrm{d}}(\hat{\boldsymbol{u}}, \hat{\boldsymbol{v}}) + \hat{b}_{\mathrm{d}}(\hat{p}, \hat{\boldsymbol{v}}) = 0 \\ \hat{b}_{\mathrm{d}}(\hat{q}, \hat{\boldsymbol{u}}) - c_{\mathrm{d}}(\hat{q}, \boldsymbol{u}) = \hat{F}(\hat{q}) \end{cases},$$

for all test functions $\boldsymbol{v}$, q, $\hat{\boldsymbol{v}}$ and $\hat{q}$ defined in their proper spaces.

2.2.2 Primal formulation

As for the equi-dimensional setting, a primal formulation can be derived by inserting Darcy's laws into the mass balance equations in (7a).

Problem 5 (Primal hybrid-dimensional strong formulation) Find p_i for $i = 1, 2$ and $\hat{p}$ such that

$$\begin{cases} -\nabla \cdot \Lambda_i \nabla p_i = f_i & \text{in } \Omega_i, \\ p_i = 0 & \text{on } \partial\Omega_i, \end{cases} \quad \text{and} \quad \begin{cases} -\nabla_{\boldsymbol{\tau}} \cdot \hat{\lambda} \nabla_{\boldsymbol{\tau}} \hat{p} = \hat{f} - [\![\Lambda \nabla p \cdot \boldsymbol{n}]\!]_{\hat{\gamma}} & \text{in } \hat{\gamma}, \\ \hat{p} = 0 & \text{on } \partial\hat{\gamma}, \end{cases} \tag{8a}$$

with interface conditions (7b-bis) reformulated as

$$\begin{cases} -\{\!\{\Lambda \nabla p \cdot \boldsymbol{n}\}\!\}_{\hat{\gamma}} = \lambda_{\hat{\gamma}} [\![p]\!]_{\hat{\gamma}} \\ -\xi_0 [\![\Lambda \nabla p \cdot \boldsymbol{n}]\!]_{\hat{\gamma}} = \lambda_{\hat{\gamma}} \left(\{\!\{p\}\!\}_{\hat{\gamma}} - \hat{p} \right) \end{cases} \quad \text{on } \hat{\gamma}. \tag{8b}$$

Proceeding to the weak formulation of the primal problem, we define the matrix bilinear form

$$a_{\mathrm{p}}(p, q) = \sum_i (\Lambda_i \nabla p_i, \nabla q_i)_{\Omega_i} + \left(\xi_0 \lambda_{\hat{\gamma}} \{\!\{p\}\!\}_{\hat{\gamma}}, \{\!\{q\}\!\}_{\hat{\gamma}} \right)_{\hat{\gamma}} + \left(\lambda_{\hat{\gamma}} [\![p]\!]_{\hat{\gamma}}, [\![q]\!]_{\hat{\gamma}} \right)_{\hat{\gamma}}$$

and the fracture bilinear form

$$\hat{a}_{\mathrm{p}}(\hat{p}, \hat{q}) = \left(\hat{\lambda} \nabla_{\boldsymbol{\tau}} \hat{p}, \nabla_{\boldsymbol{\tau}} \hat{q} \right)_{\hat{\gamma}} + (\xi_0 \lambda_{\hat{\gamma}} \hat{p}, \hat{q})_{\hat{\gamma}}.$$

The coupling between matrix and fracture is accounted for by the bilinear form

$$c_{\mathrm{p}}(p, \hat{q}) = \left(\xi_0 \lambda_{\hat{\gamma}} \{\!\{p\}\!\}_{\hat{\gamma}}, \hat{q} \right)_{\hat{\gamma}}.$$

This allows to obtain the weak formulation of Problem 5.

Problem 6 (Primal hybrid-dimensional weak formulation) Find p_i for $i = 1, 2$ and $\hat{p}$ respecting the given boundary conditions such that

$$\begin{cases} a_{\mathrm{p}}(p, q) - c_{\mathrm{p}}(q, \hat{p}) = F(q) \\ -c_{\mathrm{p}}(p, \hat{q}) + \hat{a}_{\mathrm{p}}(\hat{p}, \hat{q}) = \hat{F}(\hat{q}) \end{cases},$$

for all test functions q and $\hat{q}$ defined in their proper spaces.

The analysis of Problem 6 is straightforward and presented in, for example, [54]. However, the situation becomes more involved if the fracture is allowed to end inside the interior of the matrix, yielding a non-Lipschitz domain Ω. A rigorous mathematical analysis of this setup is carried out in [39].

2.3 Branching and intersections

In this part, we present several strategies to model the intersection of fractures. This is an important aspect, since the complex nature of networks of possibly heterogeneous fractures requires an appropriate treatment to avoid un-physical results. In a crossing, however, the different properties of every fracture branch can overlap and a unique association of properties is not always possible, so that, in general, new properties have to be defined for the crossing area, based on physical arguments to be provided by the modeler. If there is a crossing of fractures with very different permeabilities, one fracture always dominates a crossing from a geological point of view. For example, if there exists a highly permeable fracture which becomes intersected over time by an almost impermeable fracture, the crossing permeability is more likely to be almost impermeable than highly conductive or averaged. It is then neither a realistic choice to always average the permeabilities in a crossing nor to neglect the connection between different fractures. In the forthcoming reduced models, to simplify the notation, we focus our attention on a single fractures intersection inside the porous domain where several fracture branches $\hat{\gamma}_k$ meet. In all the subsequent cases, the model for the flow in the fractures, in the surrounding rock matrix and the coupling conditions between each fracture and the corresponding portion of the rock matrix are the same as in (7), or equivalently (8), but separately for all the pieces. The reduction process, similarly to the previous part, replaces the equi-dimensional domain, which represents the intersecting region, to a single point, which is $\boldsymbol{i}_p := \bigcap_{k=1}^{n_\mathrm{f}} \hat{\gamma}_k$ with n_f the number of participating branches, and introduce a new variable $\hat{p}_I$ which represents the pressure in the intersection.

The equi-dimensional setting for a crossing is shown in Figure 3 on the example of four intersecting fracture branches. The equi-dimensional model domain can be decomposed into three different domain types: matrix, fracture and crossing, namely

$$\mathcal{D} = \left(\bigcup_i \Omega_i\right) \cup \left(\bigcup_i \Gamma_i\right) \cup I.$$

We define the crossing area I with boundaries to the fractures (solid red lines) and boundaries to the rock matrix (dashed red lines), respectively as

$$(\partial I)_{\mathrm{f},i} := \partial\Gamma_i \cap \partial I \quad \text{and} \quad (\partial I)_\mathrm{m} := \partial I \backslash (\bigcup_i \partial\Gamma_i).$$

Introducing the green boundaries in Figure 4 by connecting the appropriate corners in our crossing region, we get a closed control area for which we can write the mass conservation equation which gives a relation between the crossing area pressure and the adjacent fracture pressures p_i. For the reduced model, mass conservation implies

$$\sum_{k=1}^{n_\mathrm{f}} \hat{\boldsymbol{u}}_k \cdot \boldsymbol{\tau}_k|_{\boldsymbol{i}_p} = f_I, \tag{9}$$

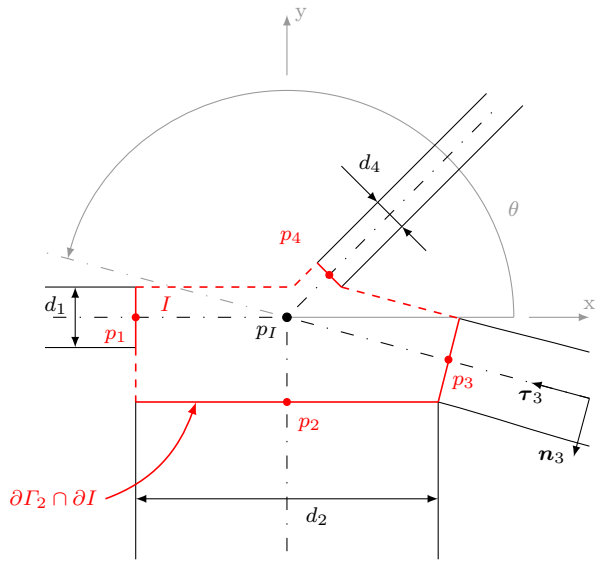

Fig. 3: Crossing with intersection geometries and location of pressure unknowns in the equidimensional model

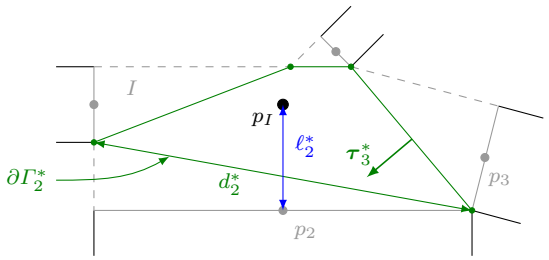

Fig. 4: Crossing with definition of geometrical parameters inside the crossing area

where $\boldsymbol{\tau}_k$ is the unit tangent along the fracture branch $\hat{\gamma}_k$, or, in other words, $\boldsymbol{\tau}_k|_{\boldsymbol{i}_p}$ is the unit outward normal of $\hat{\gamma}_k$ at $\boldsymbol{i}_p$. Moreover, $f_I \in \mathbb{R}$ is an integrated source term given for the intersection.

In the following, we will distinguish three different approaches for assigning boundary/coupling conditions for the fracture branches $\hat{\gamma}_k$ at the intersection point $\boldsymbol{i}_p$. The first two admit rather general intersection situations and are mainly suited for the primal formulation in connection with assigning degrees of freedom in the intersection point for every fracture branch: assuming pressure continuity and Robin-type conditions. The third assumes an X-shaped intersection of four fracture branches and is especially tailored for the dual formulation in connection with a lower-dimensional XFEM approach to capture the discontinuity in the intersection.

2.3.1 Assuming pressure continuity

If the properties, e.g., permeability and aperture, of the fractures and in the intersection are equal, or at least comparable, a simple strategy is to impose a pressure and normal flux continuity. The model is valid also if we can consider the intersection as a void space, i.e., infinite permeability, or small enough that it can be neglected. In the latter case the source term at the intersection may be omitted. Following [3,5,10] and the references therein, we require mass conservation (9) together with pressure continuity

$$\hat{p}_k|_{\boldsymbol{i}_p} = \hat{p}_I \quad \forall k = 1, \dots, n_\mathrm{f}. \tag{10}$$

With (9) and (10), it is possible to eliminate the value $\hat{p}_I$ of the pressure at the intersection. Moreover the primal formulation of (10) is straightforward. In some cases the heterogeneity between fractures could be severe and the aforementioned model behaves poorly, see [28].

2.3.2 Robin boundary conditions

In [55], an alternative to requiring pressure continuity in the intersection has been proposed which amounts to replace the Dirichlet-type coupling (10) by Robin-type conditions for each fracture branch.

Considering the equi-dimensional setup from Figures 3 and 4, we assume that the Darcy velocity $\boldsymbol{u}_k$ associated with the fracture branch Γ_k can be prolongated to the intersection region I and be defined there as

$$\boldsymbol{u}_k|_I = -\Lambda_I \boldsymbol{\tau}_k \frac{1}{\ell_k^*}(p_I - p_k),$$

where ℓ_k^* is the distance between the crossing point $\boldsymbol{i}_p$ and the point $\partial\Gamma_k \cap \hat{\gamma}_k$. Proceeding to the reduced model and integrating along the green lines in Figure 4 yields the Robin boundary condition

$$\hat{\boldsymbol{u}}_k \cdot \boldsymbol{\tau}_k|_{\boldsymbol{i}_p} = \boldsymbol{\tau}_k^{*\top} \Lambda_I \boldsymbol{\tau}_k \frac{d_k^*}{\ell_k^*}(\hat{p}_k - \hat{p}_I), \tag{11}$$

where $d_k^* = |\partial\Gamma_k^*|$ is the length of the interface (green) for fracture k within I and $\boldsymbol{\tau}_k^*$ the unit outward normal on that interface.

The mass conservation (9) can be rewritten as

$$\sum_{k=1}^{n_\mathrm{f}} \boldsymbol{\tau}_k^{*\top} \Lambda_I \boldsymbol{\tau}_k \frac{d_k^*}{\ell_k^*}(\hat{p}_k - \hat{p}_I) = f_I. \tag{12}$$

Conditions (11) and (12) can be easily incorporated into the primal hybrid-dimensional problem formulation (8).

2.3.3 Dual formulation for X-shaped intersections

In the case of two intersecting fractures with an X-shaped intersection, a mathematically rigorous derivation of coupling conditions is presented in [28,37]. These conditions are perfectly suited for incorporation into a dual problem formulation discretized by XFEM. In this case, we have $n_\mathrm{f} = 4$ but we make an explicit use of the fact that two distinct fractures intersect and associate only one index k with the two branches of one fracture, see Figure 5. This allows to formulate for a quantity $\hat{q}_k$ associated with fracture k its average $\{\!\{\hat{q}_k\}\!\}_{\boldsymbol{i}_p}$ and jump $[\![\hat{q}_k]\!]_{\boldsymbol{i}_p}$ at the intersection point $\boldsymbol{i}_p$. The model takes into account the aperture, permeability and angle at the intersection between fractures as well as the permeability in the intersecting region. This model allows a pressure and Darcy velocity discontinuity across the intersection, where the jumps are computed accounting for the pressure and fluxes from both fractures. In addition to the mass conservation (9), the coupling conditions are

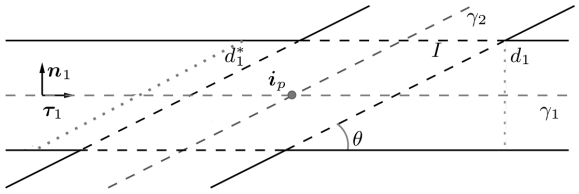

Fig. 5: Geometry and notation for the case of X-shaped intersections.

$$\begin{cases} \dfrac{|I|}{d_i} \displaystyle\sum_{k=1}^{2} \frac{\hat{\eta}_{ik}}{d_k^*} \{\!\{\hat{\boldsymbol{u}}_k \cdot \boldsymbol{\tau}_k\}\!\}_{\boldsymbol{i}_p} = [\![\hat{p}_i]\!]_{\boldsymbol{i}_p} \\ \hat{\xi}_0 \dfrac{d_j}{d_i} \hat{\eta}_{ii} [\![\hat{\boldsymbol{u}}_i \cdot \boldsymbol{\tau}_i]\!]_{\boldsymbol{i}_p} = \{\!\{\hat{p}_i\}\!\}_{\boldsymbol{i}_p} - \hat{p}_I \end{cases} \qquad \text{for } i,j = 1,2, i \neq j, \tag{13}$$

where $d_k^* = d_k / \sin\theta$ and θ is the angle between the two fractures, $\hat{\eta}_{ij}$ is the tangential projection along $\hat{\gamma}_j$ and then $\hat{\gamma}_i$ of the inverse of the permeability in the intersection region, namely $\hat{\eta}_{ij} := \boldsymbol{\tau}_i^\top \Lambda_I^{-1} \boldsymbol{\tau}_j$. Note the similarity of (13) to the interface conditions (7b-bis) of the "full" dual hybrid-dimensional problem. This allows to directly apply the corresponding XFEM techniques in a lower-dimensional context. Moreover, the system of equations (13) can be viewed as a generalization of (10) since the former boils down to the latter providing the intersection permeability goes to infinity or the dimension of the intersection goes to zero.

2.4 Boundary conditions

This section is divided into two parts: Dirichlet boundary conditions for a matrix boundary that is intersected by fractures and conditions for fracture tips that are located in the interior of the matrix domain.

2.4.1 Dirichlet conditions for fractured porous media

Boundary conditions for fractured porous media systems with explicitly modeled fractures are not easy to define. The simplest choice is to prescribe a constant pressure along a domain boundary or a linear change, for example for the case of a hydrostatic pressure distribution. This often does not reflect the highly heterogeneous structure in the case of fractured porous media systems. That again leads to a strong influence of the boundary conditions on the solution if the domain is not chosen large enough. For field scale simulations, one usually obtains pointwise pressure information from which the best boundary conditions are to be picked. In [55], a possibility is presented to interpolate pointwise pressure data along a given boundary including the information of the geometrical position and geological parameters (aperture, permeability) of the fractures intersecting with this boundary.

In particular, the situation depicted in Figure 6 is considered. For a bound-

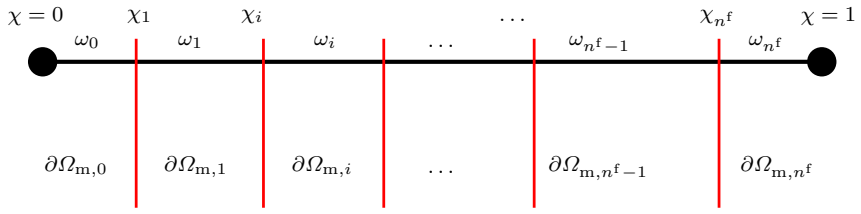

Fig. 6: Partitioning of the boundary according to intersecting fractures.

ary segment $\omega \subset \partial\Omega$ that is parametrized by $\chi \in [0,1]$, the left and right pressure values p_{left} and p_{right} at $\chi = 0$ and $\chi = 1$ are assumed to be known. The segment ω is intersected by n^f fractures that divide it in $n^\mathrm{f}+1$ parts ω_i. The goal is to find a pressure distribution p_b on ω that accounts for the presence of the intersecting fractures by admitting jumps across the fracture-boundary intersections χ_j. Proceeding analogously to the derivation of Problem 6, one has to find p_b such that $p_\mathrm{b}(0) = p_{\text{left}}$, $p_\mathrm{b}(1) = p_{\text{right}}$ and

$$\sum_{i=0}^{n^\mathrm{f}} (\lambda_{\mathrm{b},i} \nabla p_\mathrm{b}, \nabla q_\mathrm{b})_{\omega_i} + \sum_{j=1}^{n^\mathrm{f}} \lambda_{\hat{\gamma}}(\chi_j) \left([\![p_\mathrm{b}]\!]_j [\![q_\mathrm{b}]\!]_j + \xi_0 (\{\!\{ p_\mathrm{b} \}\!\}_j - p_{\mathrm{f}\,j}) \{\!\{ q_\mathrm{b} \}\!\}_j \right) = 0, \tag{14}$$

for all test functions q_b. Here, $\lambda_{\mathrm{b},i} = \boldsymbol{\tau}_\mathrm{b}^\top \Lambda_i \boldsymbol{\tau}_\mathrm{b}$ is the permeability along the boundary segment, while $[\![\cdot]\!]_j$ and $\{\!\{ \cdot \}\!\}_j$ refer to the jump and average in the fracture-boundary intersection χ_j. In order to derive a closed system, one is left with the choice of the fracture pressures $p_{\mathrm{f}\,j}$. In [55], two options are discussed. The first one assumes $p_{\mathrm{f}\,j} = \{\!\{p_\mathrm{b}\}\!\}_j$ such that the fracture pressures are indeed an outcome of solving (14). The second one builds upon expert knowledge to describe explicit values for $p_{\mathrm{f}\,j}$.

In order to facilitate the solution of (14), it is assumed that p_b is piecewise linear with respect to the unfractured parts ω_i, namely,

$$p_\mathrm{b}(\chi) = m_i \chi + b_i \text{ on } \omega_i, \tag{15}$$

with the two unknown coefficients m_i, b_i. By choosing appropriate test functions q_b, analytical expressions for these coefficients are derived for an arbitrary number of fractures and the case $p_{\mathrm{f}\,j} = \{\!\{p_\mathrm{b}\}\!\}_j$, see [55].

For example, for one single fracture, $n^\mathrm{f} = 1$, the slopes are given by

$$m_0 = \frac{\mathrm{p}_\mathrm{right} - \mathrm{p}_\mathrm{left}}{\frac{\lambda_{\mathrm{b},0}}{\lambda_{\hat{\gamma}}} + |\omega_1| + |\omega_0| \frac{\lambda_{\mathrm{b},0}}{\lambda_{\mathrm{b},1}} + (\frac{\lambda_{\mathrm{b},0}}{\lambda_{\mathrm{b},1}} - 1)},$$
$$m_1 = \frac{\mathrm{p}_\mathrm{right} - \mathrm{p}_\mathrm{left}}{\frac{\lambda_{\mathrm{b},1}}{\lambda_{\hat{\gamma}}} + |\omega_0| + |\omega_1| \frac{\lambda_{\mathrm{b},1}}{\lambda_{\mathrm{b},0}} + (1 - \frac{\lambda_{\mathrm{b},1}}{\lambda_{\mathrm{b},0}})}.$$

In [55], the resulting boundary conditions are shown to be superior to standard choices. In particular, the transition from the inner part of the domain to the boundary appears much more natural in the presence of blocking fractures.

2.4.2 Boundary and coupling conditions for fracture tips

We consider now the situation where parts of the fractures are ending inside the interior of the matrix domain, namely, in $\hat{\gamma}_\mathrm{tip} = \partial\hat{\gamma} \cap \Omega$. Apart from being challenging from the mathematical and numerical point of view, the modeling question is what kind of boundary or coupling conditions should be prescribed at $\hat{\gamma}_\mathrm{tip}$.

An obvious easy choice is to prescribe no-flow conditions across the fracture tip [7], namely,

$$\hat{\boldsymbol{u}} \cdot \boldsymbol{\tau}|_{\hat{\gamma}_\mathrm{tip}} = 0. \tag{16}$$

In many situations, this condition is well justified by the essential modeling assumption that the fracture aperture d is small compared to its lateral dimensions. However, there can be problem settings where (16) may not be accurate enough. In particular, if the tangential permeability of the fracture is larger than the normal one, namely, $\hat{\lambda} > \lambda_{\hat{\gamma}}$, the flow across the fracture tip could be rather large compared to the flow over the fracture's lateral boundaries and should be taken into consideration.

Taking into account the flow across the tip can be achieved by assigning a corresponding source term f_Ω for the matrix domain [54],

$$f_\Omega = \delta_{\hat{\gamma}_{\text{tip}}} \hat{\boldsymbol{u}} \cdot \boldsymbol{\tau}|_{\hat{\gamma}_{\text{tip}}}. \tag{17}$$

The coupling condition (17) can be complemented by a condition involving the matrix and fracture pressures. For example, one could aim for

$$\hat{p}|_{\hat{\gamma}_{\text{tip}}} = [\![p]\!]_{\hat{\gamma}_{\text{tip}}}. \tag{18}$$

Conditions (17) and (18) are discussed and investigated for the discretized primal formulation in [54]. While (17) is implemented as a source for the matrix domain, (18) can be realized as a Dirichlet condition for the fracture. However, a proper mathematical derivation from the continuous setting as well as thorough numerical comparisons with (16) are still missing.

3 Numerical discretization by means of XFEM

Before we present the numerical approximation of the previous reduced models, both in dual and primal form, using the extended finite element method (XFEM), we provide a very brief overview of its historical development and some pointers to the literature.

Ideally, one would want to use a mesh that is as structured and axis-aligned as possible. The standard Galerkin finite-element method, however, cannot handle discontinuities in the solution except by resolving them through the grid, namely, by doubling and decoupling the degrees of freedom along the discontinuities. Coming from the structural-mechanics problem of evolving cracks that leads to discontinuities in the solution (displacement, stress, strain), an extension to the standard finite-element scheme was developed, [23,24,48], and called "eXtended Finite Element Method."

From the more theoretical point, Nitsche's method, intentionally developed to handle Dirichlet constraints, evolved to a new possibility to treat interface problems, [41,43,17]. XFEM and Nitsche's method applied to interface problems are in this case essentially the same approach. An overview of recent problems where XFEM methods are investigated is given in [1]. Some works that influence the following presentation are [24,42,48]. XFEM was first used in the fractured porous media context in [20,33] for lower dimensional fractures introducing a discontinuous solution in the matrix, in [11] for lower dimensional fracture networks having different permeabilities in the network and therefore also discontinuities, and in [45] for thin heterogeneities (equidimensional) which are not resolved directly with the grid but rather with the XFEM.

In the literature such techniques are very often referred to as "partition-of-unity" PUFEM and "generalized finite-element methods" GFEM. The difference here is that those are usually on a global level where XFEM adopts the same techniques on an element-local formulation. The composite finite element method, first presented in [38], is a special type of a geometric multi-grid methods and falls therefore in the category of multi-scale methods.

3.1 Modification and addition of basis functions

In the classical Galerkin finite-element approach, the discrete solution, $p_h(\boldsymbol{x})$, at a global point $\boldsymbol{x}$ in space, which lies within an element E, is defined by the sum over all shape functions associated with this element multiplied by the value of the corresponding degree of freedom $\tilde{p}_i$, cf. for example [14],

$$p_h(\boldsymbol{x}) = \sum_{i \in \mathsf{N}^E} b_i(\boldsymbol{x})\, \tilde{p}_i. \tag{19}$$

Here, b_i denotes the shape function of the degree of freedom i, $\mathsf{N}^E = \{\mathsf{n}_1, \ldots, \mathsf{n}_\mathrm{r}\}$ denotes the set of standard degrees of freedom of the element E. All matrix elements which are not cut by a fracture are treated with such a standard finite element approach.

If an element E is cut by a fracture, additional degrees of freedom $\tilde{p}^\mathrm{e}_j$ are introduced. Those elements which are cut by at least one fracture are called enriched elements. The discrete solution on an enriched element E can be written as

$$p_h(\boldsymbol{x}) = \sum_{i \in \mathsf{N}^E} b_i(\boldsymbol{x})\, u^\mathrm{s}_i(\boldsymbol{x})\, \tilde{p}_i + \sum_{j \in \mathsf{N}^{\mathrm{e},E}} b^\mathrm{e}_j(\boldsymbol{x})\, u^\mathrm{e}_j(\boldsymbol{x})\, \tilde{p}^\mathrm{e}_j \tag{20}$$

Here, $\mathsf{N}^{\mathrm{e},E}$ is the set of enriched degrees of freedoms. To capture discontinuities in the solution the basis functions are multiplied by discontinuous functions, where u^s_i denotes the discontinuity functions for the standard degrees of freedom, while u^e_j denotes the discontinuity functions for the enriched degrees of freedom, respectively. These functions will be defined below.

In the course of this work, the standard basis at cut elements is chosen to be same as for uncut elements, i.e., (bi-)linear and the additional shape-functions are chosen to be of the same type as the standard shape-functions, i.e., also (bi-)linear, $b_i = b^\mathrm{e}_j$ if i and j refer to degrees of freedom located at the same vertex. Then, b^e_j denotes the nodal shape function of an enriched node j. Furthermore, the XFEM concept is here used in combination with the Ritz-Galerkin approach, i.e., the basis-function space and the test-function space are equal.

The choice of the discontinuity functions is somehow arbitrary, as long as certain conditions are fulfilled. One commonly desired goal is to choose the discontinuity functions such that the resulting enriched basis functions are forced to be zero in all nodes. On the one hand this leads to a propitious quality: the nodal interpolation is still guaranteed by the solution in the standard nodes alone, [48]. More importantly this property yields to enriched basis functions which are completely local with respect to the cut elements and every basis function has only one discontinuity (within this element) for every set of additional degrees of freedom. This avoids blending elements, [29], which have to be introduced otherwise. However, this is only valid for the special case of a single interface per element. The general, more complex case of several (intersecting) interfaces is more demanding and discussed in, for example, [54].

There are many other possible choices for the discontinuity functions with different properties. For example, they can be chosen such that the standard basis remains unmodified and the discontinuity is only represented by the enriched basis or such that the mean of the enriched basis functions is zero.

To become more explicit, we define the discontinuity functions by using the sign function sgn which is positive one on the side of the positive normal direction and negative one on the other, as

$$u_i^{\mathrm{s}}(\boldsymbol{x}) \coloneqq \frac{1}{2}\left|\operatorname{sgn}(\boldsymbol{x}) + \operatorname{sgn}(\boldsymbol{x}_i)\right|, \quad u_i^{\mathrm{e}}(\boldsymbol{x}) \coloneqq \frac{1}{2}\left|\operatorname{sgn}(\boldsymbol{x}) - \operatorname{sgn}(\boldsymbol{x}_i)\right|.$$

The second term, $\operatorname{sgn}(\boldsymbol{x}_i)$, associates a constant value to every node, so that the discontinuity function for the original degrees of freedom is one if $\boldsymbol{x}$ and $\boldsymbol{x}_i$ lie on the same side of the interface and zero if they are on different sides, and vice versa for the additional degrees of freedom. The modified basis functions for this kind of discontinuity functions are exemplarily shown for the one-dimensional case in Figure 7. For this approach, the orientation of the normal vector $\boldsymbol{n}$ of the interface has to be chosen. This choice is arbitrary.

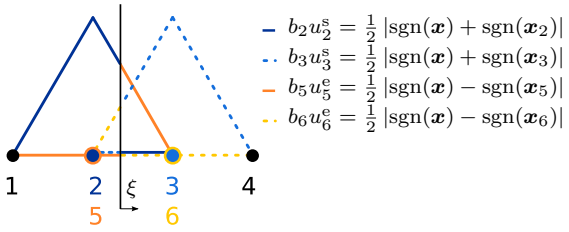

Fig. 7: The zero dimensional fracture with local coordinate ξ divides the one dimensional matrix element. Solid lines show the two modified basis functions associated to node two (degrees of freedom two and five), dashed lines the modified basis of degrees of freedom three and six at node three.

3.2 Primal formulation with XFEM

The matrix domain Ω is discretized by n^{m} triangular or quadrilateral elements E^j into $\mathsf{T}_{\mathrm{m}}^h = \{E^j\}_{j=1}^{n^{\mathrm{m}}}$ independent of γ. The fracture γ is discretized with lower-dimensional elements, $\mathsf{T}_{\mathrm{f}}^h = \{E_{\mathrm{f}}^j\}_{j=1}^{n^{\mathrm{f}}}$, independent of $\mathsf{T}_{\mathrm{m}}^h$. We define all elements $E \in \mathsf{T}_{\mathrm{m}}^h$ which are totally in or partly belonging to Ω_i as $E_i = E \cap \Omega_i$. All elements which are not fully included in one sub-domain belong to both. The discrete space can then be defined as

$$\mathcal{Q}_i^h = \{q_{h,i} \in C^0(\Omega_i) : q_{h,i}|_{E\cap\Omega_i} \in \mathbb{Q}_1(E_i),\ E \in \mathsf{T}_{\mathrm{m}}^h\}$$

for quadrilateral elements E, with $\mathbb{Q}_1$ being replaced by $\mathbb{P}_1$ for triangular elements. The complete discrete space for the rock matrix domain is then

just the product space of the sub-domain spaces $\mathcal{Q}_{\mathrm{m}}^h = \mathcal{Q}_1^h \times \mathcal{Q}_2^h$, where the elements cut by a fracture are contained twice but each with the cut basis. The discrete space for γ reads

$$\mathcal{Q}_{\mathrm{f}}^h = \{\hat{q}_h \in C^0(\gamma) : \hat{q}_h|_{E_{\mathrm{f}}} \in \mathbb{Q}_1(E_{\mathrm{f}}), E_{\mathrm{f}} \in \mathsf{T}_{\mathrm{f}}^h\}$$

so that the combined space is $\mathcal{Q}^h = \mathcal{Q}_{\mathrm{m}}^h \times \mathcal{Q}_{\mathrm{f}}^h$. This allows to obtain the discrete formulation of Problem 6.

Problem 7 (Primal hybrid-dimensional discrete formulation) Find $p_h = (p_{h,1}, p_{h,2})$ and $\hat{p}_h$ in subspaces of $\mathcal{Q}_{\mathrm{m}}^h$ and $\mathcal{Q}_{\mathrm{f}}^h$ that respect the given boundary conditions such that

$$\begin{cases} a_{\mathrm{p}}(p_h, q_h) - c_{\mathrm{p}}(q_h, \hat{p}_h) = F(q_h) \\ -c_{\mathrm{p}}(p_h, \hat{q}_h) + \hat{a}_{\mathrm{p}}(\hat{p}_h, \hat{q}_h) = \hat{F}(\hat{q}_h) \end{cases},$$

for all test functions q_h and $\hat{q}_h$ defined in proper subspaces of $\mathcal{Q}_{\mathrm{m}}^h$ and $\mathcal{Q}_{\mathrm{f}}^h$.

3.3 Dual mixed formulation

In [20], and in some more recent works such as [31,32,34] the XFEM is applied to the dual mixed formulation of the problem in a similar way, but with different FEM spaces. In particular, the lowest order Raviart-Thomas pair $\mathbb{RT}_0, \mathbb{P}_0$, see [51,53], is employed for velocity and pressure, respectively. This is a common choice in porous media simulations, which guarantees local mass conservation. In the aforementioned works the domain is discretized by means of a triangular or tetrahedral grid, however, the method could be generalized to the case of quadrilateral or hexahedral grids.

The cut mixed finite element spaces can be defined as follows. For each element E_{m} let $\mathbb{RT}_0(E_{\mathrm{m},i}) = \left\{\mathbf{v}_h|_{E_{\mathrm{m},i}} : \mathbf{v}_h \in \mathbb{RT}_0(E_{\mathrm{m}})\right\}$ be the restriction of the standard $\mathbb{RT}_0$ functions to the sub-element $E_{\mathrm{m},i}$, and analogously let $\mathbb{P}_0(E_{\mathrm{m},i}) = \left\{q_h|_{E_{\mathrm{m},i}} : q_h \in \mathbb{P}_0(E_{\mathrm{m}})\right\}$ be the restriction of the standard $\mathbb{P}_0$ functions. See Figure 8 for a sketch of the restricted basis functions and the corresponding degrees of freedom in the 2D case.

The discrete velocities and pressure in Ω are then sought in the following spaces respectively:

$$\mathbf{V}_h = \mathbf{V}_{1,h} \times \mathbf{V}_{2,h} \quad Q_h = Q_{1,h} \times Q_{2,h}$$

where

$$\mathbf{V}_{i,h} = \left\{\mathbf{v}_h \in \mathbf{H}_{div}(\Omega_i) : \mathbf{v}_h \in \mathbb{RT}_0(E_{\mathrm{m},i})\ \forall E_{\mathrm{m}} \in \mathrm{T}_{\mathrm{m}}^h\right\}$$
$$Q_{i,h} = \left\{q_h \in L^2(\Omega_i) : q_h \in \mathbb{P}_0(E_{\mathrm{m},i})\ \forall E_{\mathrm{m}} \in \mathrm{T}_{\mathrm{m}}^h\right\}.$$

The finite element spaces for the fracture problem, on γ, are the standard $\mathbb{RT}_0$-

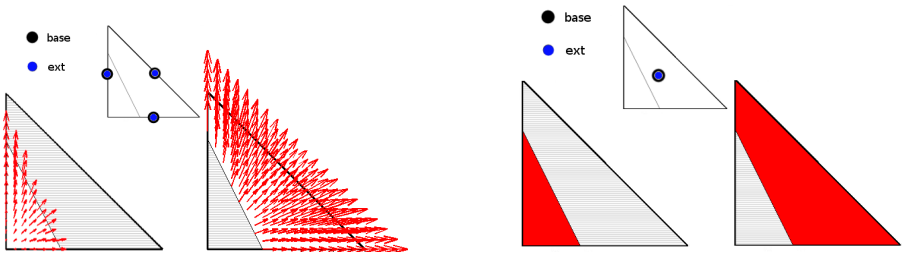

Fig. 8: Basis functions for the lowest order Raviart-Thomas pair, restricted to the subdomains Ω_i.

$\mathbb{P}_0$ in $N-1$ dimensions, thus, the discrete flux and pressure in the fracture are sought in the spaces

$$\hat{\mathbf{V}}_{i,h} = \left\{\hat{\mathbf{v}}_h \in \mathbf{H}_{div}(\gamma) : \hat{\mathbf{v}}_h \in \mathbb{RT}_0(E_\mathrm{f})\ \forall E_\mathrm{f} \in \mathsf{T}_\mathrm{f}^h\right\}$$
$$\hat{Q}_{i,h} = \left\{\hat{q}_h \in L^2(\gamma) : \hat{q}_h \in \mathbb{P}_0(E_\mathrm{f})\ \forall E_\mathrm{f} \in \mathsf{T}_\mathrm{f}^h\right\}.$$

In the case of intersecting fractures, one could consider non-matching fracture grids at the intersection: in this case, a suitable XFEM enrichment should be considered also in the fractures. We refer to [28] for details.

We can now define $\tilde{\mathbf{V}}_h = \mathbf{V}_h \times \hat{\mathbf{V}}$, and $\tilde{Q}_h = Q_h \times \hat{Q}_h$, and $\mathbf{W}_h = \tilde{\mathbf{V}}_h \times \tilde{Q}_h$ and formulate the discrete version of Problem 4.

Problem 8 (Dual hybrid-dimensional discrete formulation) Find $(\mathbf{u}_h, \hat{u}_h, p_h, \hat{p}_h) \in \mathbf{W}_h$ such that

$$a_h(\mathbf{u}_h, \hat{\mathbf{u}}_h, \mathbf{v}_h, \hat{\mathbf{v}}_h) + b_h(p_h, \hat{p}_h, \mathbf{v}_h, \hat{\mathbf{v}}_h) - b_h(q_h, \hat{q}_h, \mathbf{u}_h, \hat{\mathbf{u}}_h) =$$
$$\mathcal{F}(\mathbf{v}_h, \hat{\mathbf{v}}_h, q_h, \hat{q}_h)\ \forall (\mathbf{v}_h, \hat{\mathbf{v}}_h, q_h, \hat{q}_h) \in \mathbf{W}_h.$$

for all test functions q_h and $\hat{q}_h$ defined in proper subspaces of $\mathcal{Q}_\mathrm{m}^h$ and $\mathcal{Q}_\mathrm{f}^h$.

The well-posedness of the dual discrete problem has been proven in [20] for the case of given pressure in the fracture, and in [22] for the fully coupled case. Particularly relevant is the problem of the inf-sup stability of the extended spaces: indeed, even if we start from a stable pair the enriched spaces could present instabilities in some particular configurations. Sufficient conditions on the fracture geometry and on the underlying grid of the porous medium are given in the two aforementioned works.

3.4 Fracture grids and approximation of the coupling terms

Once the finite element spaces for both the fracture and the rock matrix are defined, one crucial ingredient is the approximation of the coupling term between the two media. To simplify the presentation, we consider only fracture and matrix grids which are *genuinely* non-matching if each fracture element

is fully contained in a N-dimensional element or is contained in a pair of facing N-dimensional elements. In the important case of matching geometries, a standard technique can be employed to approximate the coupling term, see for example [30]. The construction of the fracture grid can be done in two different ways. One possibility is to consider the fracture grid induced by the intersection between the background mesh and the interface. This approach avoids the construction of complex interpolation operators, explained in the sequel, but can be done easily only in the two-dimensional case and may produce elements with strongly varying aspect ratios. One possibility to overcome these difficulties consists in using the trace of higher dimensional basis functions as in the Trace FEM method, coupled with suitable stabilizations, see [49,47,16]. To allow a higher flexibility in the numerical discretization, it is possible to introduce an interpolation operator $\mathcal{M} : \hat{Q}_h \to Q_h$ which maps the value of the pressure in the fracture elements to the corresponding element in the matrix grid. Note that it has to take into account also fractions of fracture elements. In the particular case of a piecewise constant approximation for pressure, following [36], the discrete version of $\mathcal{M}$ is a rectangular matrix $\mathcal{M}_h$ with entries

$$[\mathcal{M}_h]_{ij} = \int_{\hat{K}_j \cap K_i} 1 \mathrm{d}x,$$

where K_i is the i-th element in matrix mesh and $\hat{K}$ is the j-th element in the fracture mesh. To preserve mass conservation at discrete level, we consider the approximation of the adjoint operator $\mathcal{M}^* : Q_h \to \hat{Q}_h$ as the transpose of $\mathcal{M}_h$.

In [30], the authors note that, in the case of an immersed fracture, if the fracture grid is too fine compared with the mesh of the matrix, depending also on the permeability contrast, the solution in the fracture could present oscillations. The authors suggest a possible explanation which is related to the singularity of the solution at the fracture tip. The aforementioned work is in the context of non-matching, but still conforming (i.e. aligned with the grid) discretizations, and the authors consider a mortar technique to deal with the non-matching elements at the interface. The same phenomenon is also observed when the XFEM method is employed. In fact considering the simple domain depicted in Figure 9, it is possible to obtain the solutions reported in Figure 10 where the fracture behaves like a barrier only in its middle part. The domain is discretized using a structured triangular mesh where each boundary edge is approximated with n segments, while the fracture is discretized using m segments. The results show that, also in the case of XFEM, the oscillations occur when the discretization of the fracture is finer than the rock mesh. Apart from cases where the mesh is too coarse the oscillations exhibit a frequency that depends only on the discretization of the outer medium. In this particular case it can be estimated as $n/2$ for most of the cases. We notice that this frequency corresponds to the $n-$th eigenfunction of the problem. Indeed, if n is odd the solution becomes asymmetrical. It is also interesting that, for fixed n, the amplitude of the oscillations is constant with increasing m, while if we

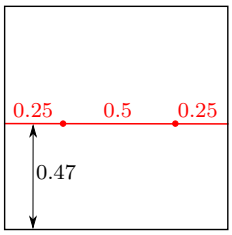

Fig. 9: Representation of the domain for the oscillation problem. In the fracture we highlight the pieces with different permeability.

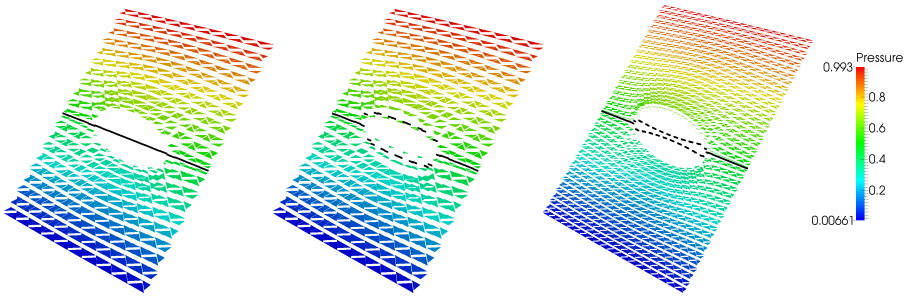

Fig. 10: In the left, the grid sizes of the matrix and the fracture are comparable. In the centre, the fracture grid is finer than the rock grid, some oscillations are present. In the right, both meshes are refined maintaining the same ratio of the grid size as the solution in the centre. In this case the amplitude of the oscillations decreases.

refine both fracture and medium the amplitude decreases. This phenomena are particularly relevant when the normal or tangential (or both) permeability change sharply along the fracture.

3.5 Basis function enrichment around fracture tips

If a fracture branch ends inside the interior of the matrix domain in the fracture tip $\hat{\gamma}_{\text{tip}}$, the question arises on how to enrich the basis functions inside an element E_{tip} that contains $\hat{\gamma}_{\text{tip}}$. For the primal formulation, an ad-hoc solution is presented and used in [54]. In E_{tip}, only those basis functions are enriched that correspond to the vertices of the element face that is intersected by the fracture, see the left picture of Figure 11. While this approach is attractive for its simplicity, it disregards the potential singularity in the solution at the tip $\hat{\gamma}_{\text{tip}}$. As described in [39], it is more appropriate to account explicitly for this singularity by adding radial functions

$$g_1(r,\theta) = \sqrt{r}\sin(\theta/2), \quad g_2(r,\theta) = \sqrt{r}\cos(\theta/2),$$

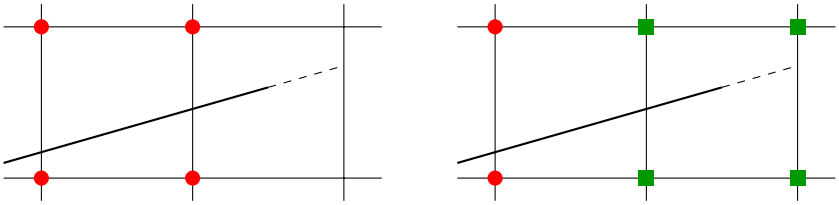

Fig. 11: Basis function enrichment around fracture tips. Red circles indicate XFEM enrichment, green squares enrichment by radial functions. Left: pure XFEM enrichment according to [54]. Right: XFEM and radial functions enrichment as suggested in [39].

multiplied with the standard basis functions b_i in E_{tip}. Here, r is the distance from $\hat{\gamma}_{\text{tip}}$, while θ indicates the angle with respect to the tangential fracture direction. This situation is depicted in the right picture of Figure 11.

4 Solvers

In this section, we discuss some issues related with the numerical solution of the system resulting from numerical discretization. In particular, we present the problem of ill-conditioning in the presence of very small sub-elements, and the possibility of using iterative strategies in a domain-decomposition framework as an alternative to a fully monolithic approach.

4.1 Conditioning

Since we are considering an arbitrary position of the interface with respect to the underlying grid, it is possible that, when an element E is cut into two sub-elments E_1, E_2, the ratio $\frac{|E_i|}{|E|}$ is very small or even zero for some elements/some configurations of the interface. The case of $|E_i| = 0$, corresponding to a fracture that contains one or two adjacent vertices of the element, is an exception ruled out by the assumptions of the XFEM method and should be handled separately, while the case of small sub-elements can lead to ill-conditioned matrices. In particular, the condition number can degenerate as $\mu(\mathsf{T}^h_{\text{m}}, \hat{\gamma}) = \min_{E\in\mathcal{G}} \min_{i=1,2} \frac{|E_i|}{|E|}$ tends to zero, where $\mathcal{G}$ denotes the set of elements that are cut by the interface. This problem has been investigated for the case of a mixed formulation in [20]. In this work, a numerical experiment is presented, where, changing the position of a vertical fracture on a structured grid, the authors obtain smaller and smaller values of $\mu(\mathsf{T}^h_{\text{m}}, \hat{\gamma})$ and compute the corresponding maximum and minimum eigenvalue of the matrix C defined as

$$C = \begin{bmatrix} A & B^T \\ -B & 0 \end{bmatrix},$$

arising from the discretization with XFEM of the Darcy problem in the cut bulk medium. While the maximum eigenvalue is approximately constant, the minimum decreases with μ. Even if the matrix is not symmetric and positive definite, the ratio between maximum and minimum eigenvalue

$$ic(C) = \frac{\max_i |\lambda_i(C)|}{\min_i |\lambda_i(C)|}$$

can be used as an indicator of ill-conditioning. In [20] an optimal preconditioner P for the problem is presented and tested on the same problem, showing that $ic(P^{-1}C)$ is constant for all μ. Moreover, a simpler diagonal preconditioner P_L can be used to perform matrix equilibration: in this case the preconditioner is not optimal with respect to the grid size h, but for a fixed h one still obtains a constant ratio $ic(P_L^{-1}C)$.

4.2 Iterative approaches

The coupled problem of flow in a porous matrix and a fracture has been interpreted in a domain-decomposition framework in [4] under the assumptions of pressure continuity across the fracture, i.e. the assumptions of permeable fractures. It is shown how, in the cases of a fracture that cuts the domain Ω in two disjoint parts Ω_i the problem can be recast as a global equation on the interface $\hat{\gamma}$ for the unknown $\hat{p}$. In a more recent work, [46], the concept is generalized to the case of fractures with arbitrary permeability, including the case of (nearly) impermeable interfaces. Once again the problem can be formulated as a positive definite problem on the interface $\hat{\gamma}$. In particular, in the case $\xi = 1$ the problem simplifies again to a problem for only one scalar unknown $\hat{p}$,

$$\overline{S}_1(\hat{p}, f_1) + \overline{S}_2(\hat{p}, f_2) + \nabla_\tau \cdot (\hat{\lambda} \nabla_\tau \hat{p}) = f_f. \tag{21}$$

where $\overline{S}_{1,2}(\hat{p}, f_{1,2})$ are the Robin-to-Neumann operators accounting for the coupling with the flow problem in $\Omega_{1,2}$. The interface equation (21) can then be solved iteratively. This approach is meant to provide an efficient method for the solution of the coupled fracture-medium problem: indeed, when considering a mixed formulation, the system is not positive definite and in realistic configurations it can be very large. Therefore, it can be convenient to eliminate some of the unknowns to obtain a problem that is easier to solve.

In the context of non-matching discretizations, an iterative approach for the solution of the coupled problem is also discussed in [20], where a similar approach is used, adding more information and numerical evidence about the convergence of the procedure. In particular, it is proven that the iterative method converges for some values of a relaxation parameter ω that must satisfy

$$\omega \gtrsim M_{\hat{\gamma}}^2 \frac{\lambda_{\hat{\gamma}}}{\xi_0 \hat{\lambda}}, \quad \text{where} \quad M_{\hat{\gamma}} = \min \left\{ 1, h \sqrt{\frac{\max\{\lambda_1, \lambda_2\}}{\lambda_{\hat{\gamma}}}} \right\}.$$

Numerical experiments show that, for small $\lambda_{\hat{\gamma}}/\hat{\lambda}$ ratios the relaxation parameter can be very small and convergence is achieved in just few iterations, while for higher ratios the iterative method converges very slowly.

In the relevant case of a discrete fracture network approximation, namely, where the rock matrix is supposed to be impervious, an interesting approach is proposed in [11,12, and references therein] to solve in an efficient way the global system of equations. The authors consider the continuous coupling conditions among the fractures, as presented in Section 2.3.1, and a primal formulation of the problem. In this part, to simplify the notation we assume that the equidimensional domain are the fractures while the one-codimensional domain are the intersections among the fractures. To decouple the solution on each fracture, the transmission conditions (10) are imposed in a weak way through an optimization problem, *i.e.* naming S a strip of intersecting elements between two fractures solve

$$\begin{cases} \min J(p) = \min \sum_{S \in \mathcal{S}} \|[\![p]\!]_S\|^2 + 2\|\{\!\{\boldsymbol{u} \cdot \boldsymbol{n}\}\!\}_S\|^2 \\ \quad s.t.\ p \text{ solution in each fracture} \end{cases}$$

where $\mathcal{S}$ is the set of all the intersection regions, the norms are defined on proper spaces and $\boldsymbol{u} \cdot \boldsymbol{n}$ is a suitable reconstruction of the normal flux at the intersection S. The optimal solution of the minimum problem gives $J(p) = 0$ and can be computed numerically using a gradient method. With this method the linear system, which couple all the fractures, has much smaller size than the aforementioned approaches and the computation of the pressure in each fracture is completely parallelizable.

5 Conclusion

In this review paper, we presented several mathematical models and numerical algorithms to simulate single-phase flow in a porous medium containing fractures. Two main challenges are addressed. First, the fractures play a crucial role in subsurface flows and should be carefully accounted for to achieve reliable simulations, however their geometrical and geological data pose several difficulties from a modeling and discrete point of view. A common approach which is broadly used in the literature is to consider an hybrid-dimensional model where the fractures are treated as objects of lower dimension. Second, the position of the fractures may be unknown and several scenarios are needed to obtain a representative solution of the problem, or to speed up the simulations: for this reason it is better to allow these fractures to be geometrically decoupled from the surrounding porous medium. In this case, an XFEM approach can be a valuable option to overcome this requests. Several geometrical difficulties have been addressed in this paper, such as the treatment of intersections and tips. To the best of our knowledge, several interesting issues are still open for further investigation, such as a full three-dimensional setting for

general networks of fractures with XFEM, a physical derivation of a more appropriate condition at the fracture tip, suitable stabilizations to increase the robustness of the linear solvers and a deep analysis for the case of vanishing aperture.

References

1. Y. Abdelaziz and A. Hamouine. A survey of the extended finite element. *Computers & structures*, 86(11-12):1141–1151, 2008.
2. C. Alboin, J. Jaffré, J. E. Roberts, and C. Serres. Modeling fractures as interfaces for flow and transport in porous media. In *Fluid Flow and Transport in Porous Media, Mathematical and Numerical Treatment: Proceedings of an AMS-IMS-SIAM Joint Summer Research Conference on Fluid Flow and Transport in Porous Media, Mathematical and Numerical Treatment, June 17-21, 2001, Mount Holyoke College, South Hadley, Massachusetts*, volume 295, pages 13–25. American Mathematical Soc., 2002.
3. C. Alboin, J. Jaffré, J. E. Roberts, and C. Serres. Modeling fractures as interfaces for flow and transport in porous media. In *Fluid flow and transport in porous media: mathematical and numerical treatment (South Hadley, MA, 2001)*, volume 295 of *Contemp. Math.*, pages 13–24. Amer. Math. Soc., Providence, RI, 2002.
4. C. Alboin, J. Jaffré, J. E. Roberts, X. Wang, and C. Serres. Domain decomposition for some transmission problems in flow in porous media. In *Numerical treatment of multiphase flows in porous media (Beijing, 1999)*, volume 552 of *Lecture Notes in Phys.*, pages 22–34. Springer, Berlin, 2000.
5. L. Amir, M. Kern, V. Martin, and J. E. Roberts. Décomposition de domaine et préconditionnement pour un modèle 3D en milieu poreux fracturé. In *Proceeding of JANO 8, 8th conference on Numerical Analysis and Optimization*, Dec. 2005.
6. P. Angot. A model of fracture for elliptic problems with flux and solution jumps. *Comptes Rendus Mathematique*, 337(6):425–430, 2003.
7. P. Angot, F. Boyer, and F. Hubert. Asymptotic and numerical modelling of flows in fractured porous media. *M2AN Math. Model. Numer. Anal.*, 43(2):239–275, 2009.
8. P. F. Antonietti, L. Formaggia, A. Scotti, M. Verani, and N. Verzotti. Mimetic finite difference approximation of flows in fractured porous media. Technical report, Politecnico di Milano, 2015.
9. J. Bear. *Dynamics of Fluids in Porous Media*. American Elsevier, 1972.
10. M. F. Benedetto, S. Berrone, S. Pieraccini, and S. Scialò. The virtual element method for discrete fracture network simulations. *Computer Methods in Applied Mechanics and Engineering*, 280(0):135–156, 2014.
11. S. Berrone, S. Pieraccini, and S. Scialò. On simulations of discrete fracture network flows with an optimization-based extended finite element method. *SIAM Journal on Scientific Computing*, 35(2):908–935, 2013.
12. S. Berrone, S. Pieraccini, and S. Scialò. An optimization approach for large scale simulations of discrete fracture network flows. *Journal of Computational Physics*, 256(0):838 – 853, 2014.
13. W. M. Bonn and J. M. Nordbotten. Robust discretization of flow in fractured porous media. arXiv:1601.06977 [math.NA], 2016.
14. D. Braess. *Finite elements: Theory, fast solvers, and applications in solid mechanics*. Cambridge University Press, 2007.
15. F. Brezzi and M. Fortin. *Mixed and Hybrid Finite Element Methods*, volume 15 of *Computational Mathematics*. Springer Verlag, Berlin, 1991.
16. E. Burman, S. Claus, P. Hansbo, M. G. Larson, and A. Massing. Cutfem: discretizing geometry and partial differential equations. *International Journal for Numerical Methods in Engineering*, 2014.
17. E. Burman and P. Hansbo. Fictitious domain finite element methods using cut elements: II. A stabilized Nitsche method. *Applied Numerical Mathematics*, 62(4):328–341, 2012.

18. C. D'Angelo and A. Scotti. A Mixed Finite Element Method for Darcy Flow in Fractured Porous Media with Non-Matching Grids. Technical report, MOX, Mathematical Department, Politecnico di Milano, 2010.
19. C. D'Angelo and A. Scotti. A mixed finite element method for Darcy flow in fractured porous media with non-matching grids. *Mathematical Modelling and Numerical Analysis*, 46(02):465–489, 2012.
20. C. D'Angelo and A. Scotti. A mixed finite element method for darcy flow in fractured porous media with non-matching grids. *ESAIM: Mathematical Modelling and Numerical Analysis*, 46(02):465–489, 2012.
21. F. Dassi, S. Perotto, L. Formaggia, and P. Ruffo. Efficient geometric reconstruction of complex geological structures. *Mathematics and Computers in Simulation*, 2014.
22. M. Del Pra, A. Fumagalli, and A. Scotti. Well posedness of fully coupled fracture/bulk darcy flow with xfem. Technical Report 25/2015, Politecnico di Milano, May 2015. Submitted to: SIAM Journal on Numerical Analysis.
23. J. Dolbow. *An extended finite element method with discontinuous enrichment for applied mechanics*. PhD thesis, Northwestern University, 1999.
24. J. Dolbow, N. Moës, and T. Belytschko. Discontinuous enrichment in finite elements with a partition of unity method. *Finite Elements in Analysis and Design*, 36(3-4):235–260, 2000.
25. A. Ern and J.-L. Guermond. *Theory and practice of finite elements*. Applied mathematical sciences. Springer, 2004.
26. I. Faille, E. Flauraud, F. Nataf, S. Pégaz-Fiornet, F. Schneider, and F. Willien. A new fault model in geological basin modelling. Application of finite volume scheme and domain decomposition methods. In *Finite volumes for complex applications, III (Porquerolles, 2002)*, pages 529–536. Hermes Sci. Publ., Paris, 2002.
27. I. Faille, A. Fumagalli, J. Jaffré, and J. E. Roberts. A double-layer reduced model for fault flow on slipping domains with hybrid finite volume scheme. In preparation for: SIAM - Journal of Scientific Computing, 2014.
28. L. Formaggia, A. Fumagalli, A. Scotti, and P. Ruffo. A reduced model for Darcy's problem in networks of fractures. *ESAIM: Mathematical Modelling and Numerical Analysis*, 48:1089–1116, 7 2014.
29. T. Fries. A corrected XFEM approximation without problems in blending elements. *International Journal for Numerical Methods in Engineering*, 75(5):503–532, 2008.
30. N. Frih, V. Martin, J. E. Roberts, and A. Saâda. Modeling fractures as interfaces with nonmatching grids. *Computational Geosciences*, 16(4):1043–1060, 2012.
31. A. Fumagalli. *Numerical Modelling of Flows in Fractured Porous Media by the XFEM Method*. PhD thesis, Politecnico di Milano, 2012.
32. A. Fumagalli and A. Scotti. Numerical modelling of multiphase subsurface flow in the presence of fractures. *Communications in Applied and Industrial Mathematics*, 3(1), 2011.
33. A. Fumagalli and A. Scotti. An efficient XFEM approximation of Darcy flows in fractured porous media. *MOX report 53*, 2012.
34. A. Fumagalli and A. Scotti. A reduced model for flow and transport in fractured porous media with non-matching grids. In *Proceedings of ENUMATH 2011, the 9^{th} European Conference on Numerical Mathematics and Advanced Applications, Springer-Verlag*, 2012.
35. A. Fumagalli and A. Scotti. A numerical method for two-phase flow in fractured porous media with non-matching grids. *Advances in Water Resources*, 62:454–464, 2013.
36. A. Fumagalli and A. Scotti. A numerical method for two-phase flow in fractured porous media with non-matching grids. *Advances in Water Resources*, 62, Part C(0):454–464, 2013. Computational Methods in Geologic CO2 Sequestration.
37. A. Fumagalli and A. Scotti. An efficient XFEM approximation of Darcy flow in arbitrarly fractured porous media. *Oil and Gas Sciences and Technologies - Revue d'IFP Energies Nouvelles*, 69(4):555–564, April 2014.
38. W. Hackbusch and S. A. Sauter. Composite finite elements for the approximation of PDEs on domains with complicated micro-structures. *Numerische Mathematik*, 75(4):447–472, 1997.
39. K. Hanowski and O. Sander. Simulation of deformation and flow in fractured, poroelastic materials. In preparation, 2016.

40. A. Hansbo and P. Hansbo. An unfitted finite element method, based on Nitsche's method, for elliptic interface problems. *Comput. Methods Appl. Mech. Engrg.*, 191(47-48):5537–5552, 2002.
41. A. Hansbo and P. Hansbo. An unfitted finite element method, based on Nitsche's method, for elliptic interface problems. *Computer methods in applied mechanics and engineering*, 191(47-48):5537–5552, 2002.
42. A. Hansbo and P. Hansbo. A finite element method for the simulation of strong and weak discontinuities in solid mechanics. *Computer methods in applied mechanics and engineering*, 193(33):3523–3540, 2004.
43. P. Hansbo. Nitsche's method for interface problems in computational mechanics. *GAMM-Mitteilungen*, 28(2):183–206, 2005.
44. H. Huang, T. A. Long, J. Wan, and W. P. Brown. On the use of enriched finite element method to model subsurface features in porous media flow problems. *Computational Geosciences*, 15(4):721–736, 2011.
45. H. Huang, T. A. Long, J. Wan, and W. P. Brown. On the use of enriched finite element method to model subsurface features in porous media flow problems. *Computational Geosciences*, 15(4):721–736, 2011.
46. V. Martin, J. Jaffré, and J. E. Roberts. Modeling fractures and barriers as interfaces for flow in porous media. *SIAM J. Sci. Comput.*, 26(5):1667–1691, 2005.
47. A. Massing, M. G. Larson, and A. Logg. Efficient implementation of finite element methods on non-matching and overlapping meshes in 3d. *arXiv preprint arXiv:1210.7076*, 2012.
48. S. Mohammadi. *Extended finite element method.* John Wiley & Sons, 2008.
49. G. J. Olshanskii MA., Reusken A. A finite element method for elliptic equations on surfaces. *SIAM Journal on Numerical Analysis*, 47(5):3339–3358, 2009.
50. A. Quarteroni and A. Valli. *Numerical approximation of partial differential equations*, volume 23 of *Springer Series in Computational Mathematics*. Springer-Verlag, Berlin, 1994.
51. P.-A. Raviart and J.-M. Thomas. A mixed finite element method for second order elliptic problems. *Lecture Notes in Mathematics*, 606:292–315, 1977.
52. E. Remij, J. Remmers, J. Huyghe, and D. Smeulders. The enhanced local pressure model for the accurate analysis of fluid pressure driven fracture in porous materials. *Computer Methods in Applied Mechanics and Engineering*, 286:296–312, 2015.
53. J. E. Roberts and J.-M. Thomas. Mixed and hybrid methods. In *Handbook of numerical analysis, Vol. II*, Handb. Numer. Anal., II, pages 523–639. North-Holland, Amsterdam, 1991.
54. N. Schwenck. *An XFEM-Based Model for Fluid Flow in Fractured Porous Media.* PhD thesis, University of Stuttgart, Department of Hydromechanics and Modelling of Hydrosystems, 2015.
55. N. Schwenck, B. Flemisch, R. Helmig, and B. Wohlmuth. Dimensionally reduced flow models in fractured porous media: crossings and boundaries. *Computational Geosciences*, 19(6):1219–1230, 2015.
56. X. Tunc, I. Faille, T. Gallouët, M. C. Cacas, and P. Havé. A model for conductive faults with non-matching grids. *Computational Geosciences*, 16:277–296, 2012.
57. R. W. Zimmerman, S. Kumar, and G. S. Bodvarsson. Lubrication theory analysis of the permeability of rough-walled fractures. *International Journal of Rock Mechanics and Mining Sciences & Geomechanics Abstracts*, 28(4):325–331, 1991.

MOX Technical Reports, last issues

Dipartimento di Matematica
Politecnico di Milano, Via Bonardi 9 - 20133 Milano (Italy)

08/2016 Dassi, F.; Perotto, S.; Si, H.; Streckenbach, T.
A priori anisotropic mesh adaptation driven by a higher dimensional embedding

09/2016 Rizzo, C.B.; de Barros, F.P.J.; Perotto, S.; Oldani, L.; Guadagnini, A.
Relative impact of advective and dispersive processes on the efficiency of POD-based model reduction for solute transport in porous media

07/2016 Pacciarini, P.; Gervasio, P.; Quarteroni, A.
Spectral Based Discontinuous Galerkin Reduced Basis Element Method for Parametrized Stokes Problems

05/2016 Alfio Quarteroni, A.; Lassila, T.; Rossi, S.; Ruiz-Baier, R.
Integrated Heart - Coupling multiscale and multiphysics models for the simulation of the cardiac function

06/2016 Micheletti, S.; Perotto, S.; Signorini, M.
Anisotropic mesh adaptation for the generalized Ambrosio-Tortorelli functional with application to brittle fracture

04/2016 Pettinati, V.; Ambrosi, D; Ciarletta P.; Pezzuto S.
Finite element simulations of the active stress in the imaginal disc of the Drosophila Melanogaster

03/2016 Tarabelloni, N.; Ieva, F.
On Data Robustification in Functional Data Analysis

02/2016 Crivellaro, A.; Perotto, S.; Zonca, S.
Reconstruction of 3D scattered data via radial basis functions by efficient and robust techniques

01/2016 Domanin, M.; Buora, A.; Scardulla, F.; Guerciotti, B.; Forzenigo, L.; Biondetti, P.; Vergara, C.
Computational fluid-dynamic analysis of carotid bifurcations after endarterectomy: closure with patch graft versus direct suture

62/2015 Signorini, M.; Zlotnik, S.; Díez, P.
Proper Generalized Decomposition solution of the parameterized Helmholtz problem: application to inverse geophysical problems.